Analysis of Pantograph Aerodynamic Loads using Computational Fluid Dynamic Studies

F. F. Jackson[1], R. Mishra[1], J. Pombo[2,3,4], P. Antunes[2,3], J.M. Rebelo[2], J. Santos[2], H. Magalhães[3]

[1]School of Computing and Engineering, University of Huddersfield, Huddersfield, United Kingdom
[2]Institute of Railway Research, School of Computing and Engineering, University of Huddersfield, Huddersfield, United Kingdom
[3]IDMEC, Instituto Superior Técnico, Universidade de Lisboa, Lisboa, Portugal
[4]ISEL, Instituto Politécnico de Lisboa, Lisboa, Portugal

Abstract

Maintaining consistent contact between the pantograph strips and the catenary wire is essential for smooth power delivery to the train. In this paper, aerodynamic loads acting on individual components of a HSX pantograph are investigated through the use of computational fluid dynamics. Both the lift and drag forces are monitored for the pantograph at three different operational heights of 320mm, 860mm, and 2100mm. With increasing height, both the total drag and lift forces are found to increase and the nature of lift force changes from providing a downward force to uplift at the maximum height tested.

Keywords: Pantograph-Catenary Interaction, Aerodynamic Forces, Computational Fluid Dynamics, Numerical Simulation.

1   Introduction

The consideration of aerodynamic forces is important for analysing the performance of pantograph-catenary systems [1]. This includes the requirements for pantograph–catenary contact force set by standards such as EN50367:2012. A baseline upward force is provided by the pantograph pneumatic actuator and, at higher speeds, aerodynamic forces become significant. If the pantograph–catenary force is too large,

there will be excessive wear on the contact strips. Alternatively, if the force is too small, an improper current collection may be established. As such, there has been considerable research interest, both experimentally and numerically in the evaluation of aerodynamic loads. While experimental methods provide a means of getting representative and reliable data, computational fluid dynamics (CFD) offers a cost-effective alternative for virtually running many different configurations and case studies. As such, this topic has been extensively analysed in a diverse range of applications [2-4].

Carnevale et al [5] used both experimental wind tunnel methods and CFD to investigate both knuckle-leading and knuckle-trailing pantographs in terms of the generated aerodynamic uplift force. Xiao et al. [6] explored the effect of platform sinking height on the aerodynamic performance of a high-speed train pantograph. Their study highlighted the importance of the "shielding" effect on dynamic uplift and drag forces. Dai et al. [7] numerically explored the influence of contact strip spacing on the pantograph head. They found that in both leading and trailing configurations the uplift and drag forces increase with increase in strip spacing. Dai et al.[8] explored the optimisation of aerodynamic uplift for both a knuckle-leading and knuckle trailing pantograph to ensure a uniform load across both orientations. Numerical investigations of aerodynamic loads both on the train and on the pantograph for trains passing through a tunnel have been explored by Niu et al. [9] and Li et al. [10] respectively. Li et al. [11] also explored aerodynamic loads on a pantograph in different configurations, including three different operational heights and two orientations, i.e. knuckle trailing and knuckle leading. However, their computational domain did not account for the sunken platform (and hence boundary layer) in which the pantograph assembly is located. In addition to aerodynamic loads, currently, there is also considerable interest in the aeroacoustics properties of pantographs [12, 13].

Although considerable research has been directed towards understanding the influence of aerodynamic loads on the pantograph, there is still a requirement to understand how the loads change for different operating heights of the pantograph in addition to effects associated with a pantograph on a realistic sunken platform. In this study, the aerodynamic loads are evaluated for individual pantograph components, for three different operating heights: low, normal, and high. The base of the pantograph is placed on a sunken platform, on a model of the train body.

2   Modelling

A HSX pantograph is considered in this investigation. An illustration of the pantograph is displayed in Figure 1 for each of the different operation heights. In this study, three different operational heights are considered and are referred to as low, normal, and high, with heights of 320mm, 860mm, and 2100mm respectively. Detailed CAD models are used, following which small geometrical features, which are assumed to have a negligible effect on the aerodynamic performance, are removed before generating the mesh.
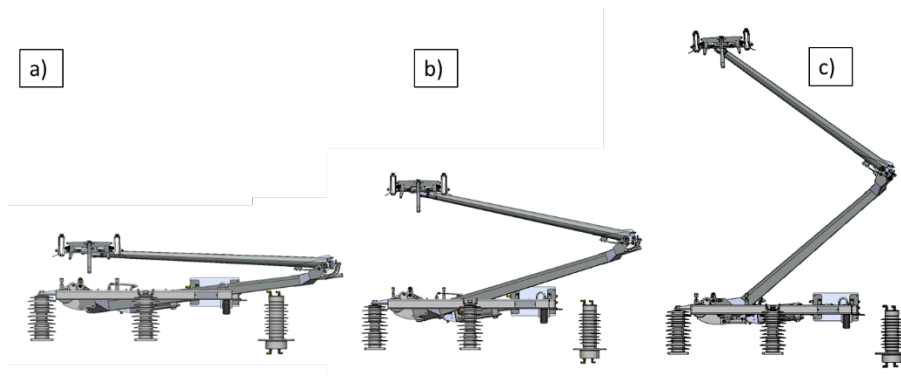
Figure 1: Geometry of HSX pantograph in a) low configuration, b) normal configuration, and c) high configuration.

The computation domain includes a simplified body for the train as well as a sunken platform in which the pantograph assembly is placed. The dimensions of the computation flow domain and applied boundary conditions are displayed in Figure 2. The inlet and moving wall velocity are both set as 200km/h.
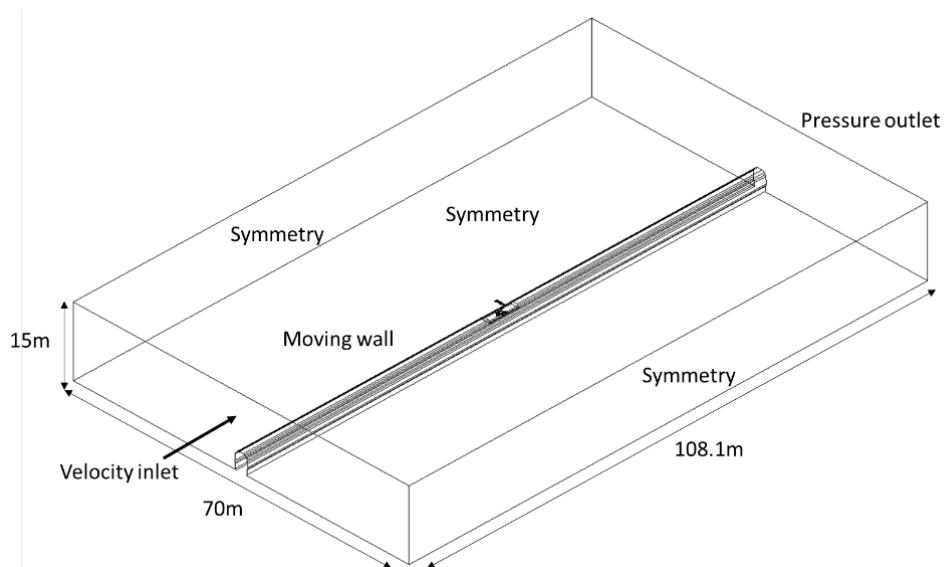
Figure 2: Details of the computation domain used for CFD analysis.

The numerical modelling assumes incompressible flow, which is valid for Mach numbers below 0.3. The Reynolds-Average Navier Stokes equations are solved in addition to the two-equation, k-ω SST [14] turbulence model using the finite volume method of discretisation.

Due to the geometric complexities of the pantograph assembly, the mesh is generated using fully tetrahedral elements. To allow for additional control, two bodies of influence are created, encapsulating the whole pantograph assembly. A mesh independence study is conducted, and the final mesh, which is deemed suitable for analysis is displayed in Figure 3 and consists of ~11 million elements.
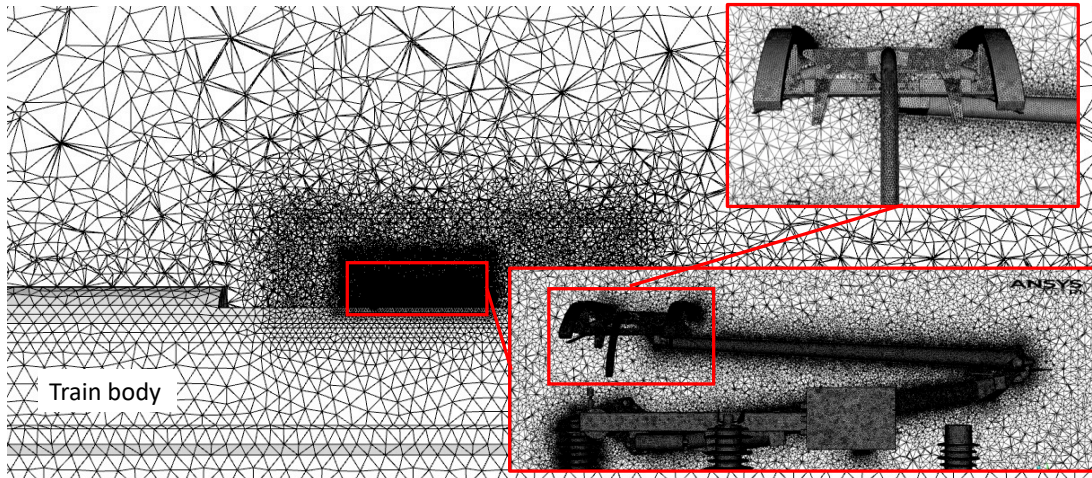
Figure 3: Illustration of generated CFD mesh with local refinement.

For each configuration, the lift and drag force on the individual pantograph components are monitored to ensure simulation convergence.

3   Results

To investigate the aerodynamic characteristics of the HSX pantograph, the pressure field surrounding the pantograph assembly is first examined, as shown in Figure 4. In Figure 4a, the pantograph is in the lowest configuration and the regions of high and low pressure surrounding the pantograph head are clearly visible. In Figure 4b, it is seen that both high- and low-pressure regions have increased. Finally, in Figure 4c, it can be seen that there is high pressure acting on both the arms as they are now almost perpendicular to the incoming flow. Additionally, there is a larger region of low pressure visible behind the knee and head.
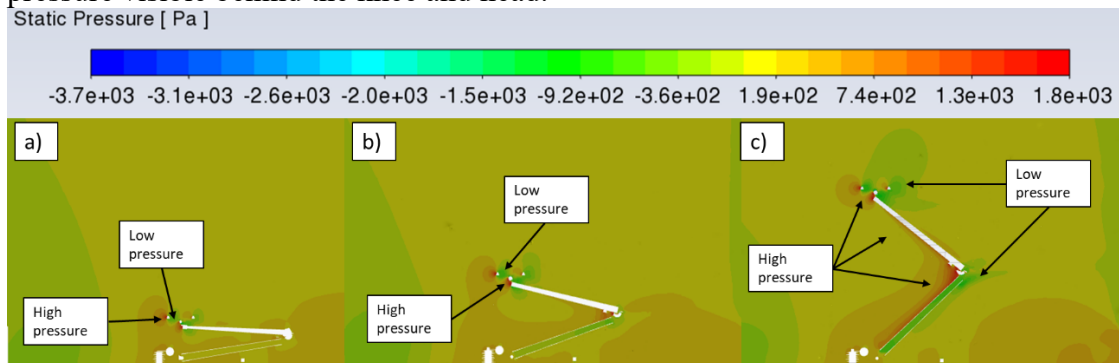
Figure 4: Pressure contours for plane cutting through the centre of the domain, for pantograph in a) low configuration, b) normal configuration and c) high configuration.

Illustrations of the pressure field downstream of the pantograph are displayed in Figure 5. Here, asymmetries in the pressure field are apparent due to the geometrical asymmetry of the pantograph assembly. Clear asymmetries are seen in Figure 5a and

4

Figure 5b for the low and normal configurations respectively. In Figure 5c, it is also clear to see spots of low pressure, which are generated by the vanes.
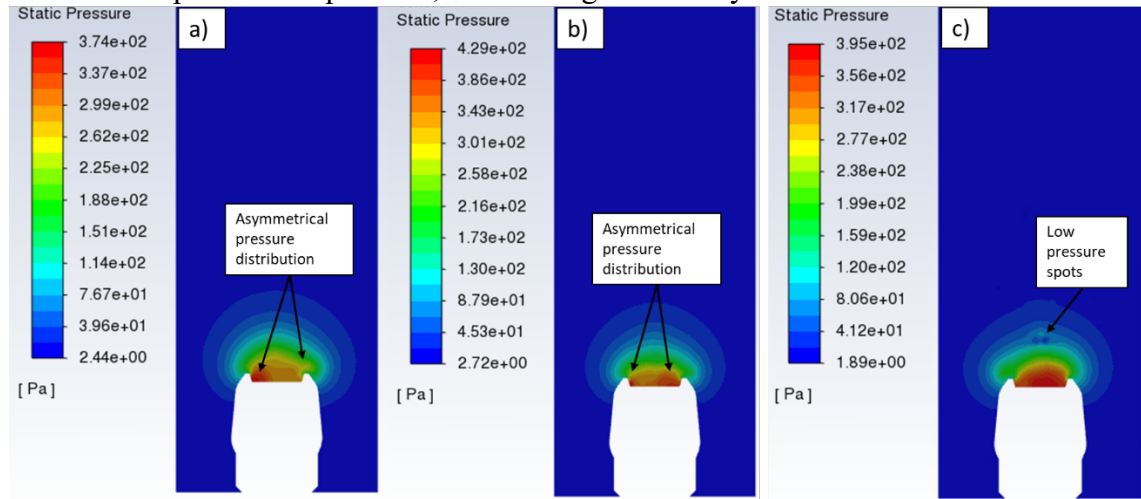
Figure 5: Static pressure contour plots on a plane perpendicular to the direction of travel (inlet velocity) 3m behind the pantograph in a) low configuration, b) normal configuration and c) high configuration.

The above discussion clearly indicates that the pressure field is highly non-uniform in the vicinity of the pantograph for all the three heights, however extent of non-uniformity increases with increasing height. To explore the flow fields further, plots of the velocity magnitude for each configuration are displayed in Figure 6. In Figure 6a, the pantograph is in the low configuration and much of the lower arm is confined within a region of low velocity magnitude due to the shielding provided by the sunken platform. In Figure 6b, it can be seen that the increase in pantograph height results in more of the components affected by the free stream velocity conditions. Finally, in Figure 6c, it is evident from the low velocity wake regions behind the knee and head region that there is a considerable modification to the free stream flow conditions, generating considerable form drag.
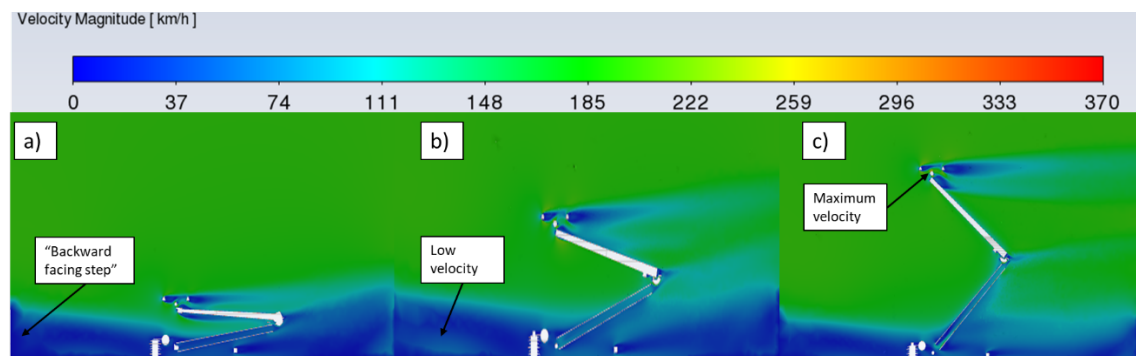
Figure 6: Velocity magnitude contour plots for plane cutting centre of the domain with pantograph in a) low configuration, b) normal configuration, and c) high configuration.

To give a quantitative description of the velocity magnitude, values at three points, separated by 2m, starting at 3m downstream of the pantograph are monitored and

displayed in Figure 7. The lines at which the velocity is measured are illustrated in Figure 7a. Note that the measurement point 'z1' is located within the sunken area where the pantograph is positioned and the remaining points start from the carriage roof. The length normalisation factor, L, is taken as the length of the line from the platform or carriage roof to the top of the computational domain and the velocity is normalised by the inlet velocity of 200km/h. As the pantograph height increases from a) to c) the variation in velocity magnitude becomes more pronounced. Furthermore, at points z2 and z3, further downstream of the pantograph, the velocity variation reduces and a normal logarithmic velocity profile is obtained.
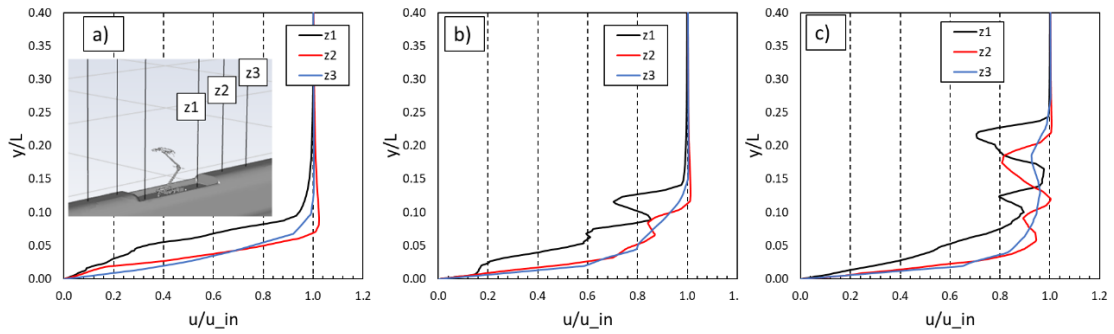
Figure 7: Normalised velocity magnitude plots for three lines placed downstream of the pantograph. Pantograph in a) low configuration, b) normal configuration and c) high configuration.

Finally, after analysis of the pressure and velocity fields, the drag and lift forces, which are caused by a combination of pressure and shear forces, for each component are computed and shown in Table 1and Table 2 respectively. The total drag force on the pantograph assembly is found to be 204.3N, 284.3N and 432.4N for the low, normal, and high configuration respectively. With a height increase from 320mm to 2100mm, the total drag force increased by over 111%. The maximum drag was experienced by the head of the pantograph for each of the three heights.

Table 1: Drag force [N] for each of the monitored pantograph components.

Configuration	Head (Inner)	Arm (Lower)	Head (Outer)	Arm (Upper)	Vanes
Low	32.4	14.0	124.4	26.9	6.6
Normal	42.2	32.8	155.0	41.4	12.9
Heigh	49.5	97.7	170.9	83.2	31.1

The total lift force on the pantograph assembly is -20N, -9.1N and 36.3N for the low, normal, and high configuration respectively. Interestingly, for the low and normal configuration, the net aerodynamic is such to generate a downward force. For the high configuration, there is a net upward force, which is primarily generated by the vanes. Typically, for all the heights, head (inner), arm (upper) and vanes provide a positive lift where as arm (lower) and head (outer) provide down force.

6

Table 2: Lift force [N] for each of the monitored pantograph components.

Configuration	Head (Inner)	Arm (Lower)	Head (Outer)	Arm (Upper)	Vanes
Low	4.9	-17.0	-21.8	1.1	12.0
Normal	22.9	-43.5	-29.0	4.1	36.4
Heigh	30.1	-84.7	-33.9	34.9	89.9

4   Conclusions and Contributions

In this paper, the aerodynamic characteristics of the HSX pantograph are investigated for three different operation heights using computational fluid dynamics. It is shown that the flow field around the pantograph is very complex and aerodynamic forces on individual pantograph components change considerably, resulting in variations in both the total drag and lift forces with change in operation height. With an increase in operation height from 320mm to 2100mm, the drag force increased by over 111% and the lift changed from initially generating a net downward force, to generating uplift.

The outcomes of this work allow to apply aerodynamic loads in realistic 3D computational studies that use a multibody approach to represent the pantograph. This methodology enables to model the individual components of the pantograph and apply on them the aerodynamic loads computed here. Such studies allow to carry out realistic operational analyses of pantograph-catenary interaction in order to improve the current collection performance and support the design of optimised systems.

Acknowledgements

References

[1]   J. Pombo, J. Ambrósio, M. Pereira, F. Rauter, A. Collina, and A. Facchinetti, "Influence of the aerodynamic forces on the pantograph–catenary system for high-speed trains," *Vehicle System Dynamics,* vol. 47, no. 11, pp. 1327-1347, 2009.

[2]   V. C. Agarwal and R. Mishra, "Optimal design of a multi-stage capsule handling multi-phase pipeline," *International Journal of Pressure Vessels and Piping,* vol. 75, no. 1, pp. 27-35, 1998, doi: 10.1016/S0308-0161(98)00003-9.

[3]   T. Asim, A. Oliveira, M. Charlton, and R. Mishra, "Improved design of a multi-stage continuous-resistance trim for minimum energy loss in control valves," *Energy,* vol. 174, pp. 954-971, 2019, doi: 10.1016/j.energy.2019.03.041.

[4]   F. J. Frankie, "Aerodynamic optimisation of formula student vehicle using computational fluid dynamics," *Fields: Journal of Huddersfield Student Research*, doi: 10.3316/informit.691941092489843.

[5]   M. Carnevale, A. Facchinetti, L. Maggiori, and D. Rocchi, "Computational fluid dynamics as a means of assessing the influence of aerodynamic forces on the mean contact force acting on a pantograph," *Proceedings of the Institution of Mechanical Engineers, Part F: Journal of Rail and Rapid Transit,* vol. 230, no. 7, pp. 1698-1713, 2016.

[6]   C. Xiao, M. Yang, C. Tan, and Z. Lu, "Effects of platform sinking height on the unsteady aerodynamic performance of high-speed train pantograph," *Journal of Wind Engineering and Industrial Aerodynamics,* vol. 204, p. 104284, 2020/09/01/ 2020, doi: https://doi.org/10.1016/j.jweia.2020.104284.

[7]   Z. Dai, T. Li, J. Deng, N. Zhou, and W. Zhang, "Effect of the strip spacing on the aerodynamic performance of a high-speed double-strip pantograph," *Vehicle System Dynamics,* pp. 1-17, 2021.

[8]   Z. Dai, T. Li, N. Zhou, J. Zhang, and W. Zhang, "Numerical simulation and optimization of aerodynamic uplift force of a high-speed pantograph," *Railway Engineering Science,* vol. 30, no. 1, pp. 117-128, 2022.

[9]   J.-q. Niu, D. Zhou, X.-f. Liang, S. Liu, and T.-h. Liu, "Numerical simulation of the Reynolds number effect on the aerodynamic pressure in tunnels," *Journal of Wind Engineering and Industrial Aerodynamics,* vol. 173, pp. 187-198, 2018/02/01/ 2018, doi: https://doi.org/10.1016/j.jweia.2017.12.013.

[10]   R. Li, W. Zhang, Z. Ning, B. Liu, D. Zou, and W. Liu, "Influence of a high-speed train passing through a tunnel on pantograph aerodynamics and pantograph–catenary interaction," *Proceedings of the Institution of Mechanical Engineers, Part F: Journal of Rail and Rapid Transit,* vol. 231, no. 2, pp. 198-210, 2017.

[11]   T. Li, W. Zhang, J. Zhang, and D. Qin, "Effects of train pantograph operating height on aerodynamic performance (in Chinese)," 2020.

[12]   A. F. AbdelGawad, N. M. Aljameel, and R. E. Shaltout, "Computational Modelling of the Aerodynamic Noise of the Full-Scale Pantograph of High-Speed Trains," *Journal of Advanced Research in Fluid Mechanics and Thermal Sciences,* vol. 93, no. 1, pp. 94-109, 2022.

[13]   Y. Zhang, J. Zhang, T. Li, and L. Zhang, "Investigation of the aeroacoustic behavior and aerodynamic noise of a high-speed train pantograph," *Science China Technological Sciences,* vol. 60, no. 4, pp. 561-575, 2017.

[14]   F. Menter, "Zonal two equation kw turbulence models for aerodynamic flows," in *23rd fluid dynamics, plasmadynamics, and lasers conference*, 1993, p. 2906.